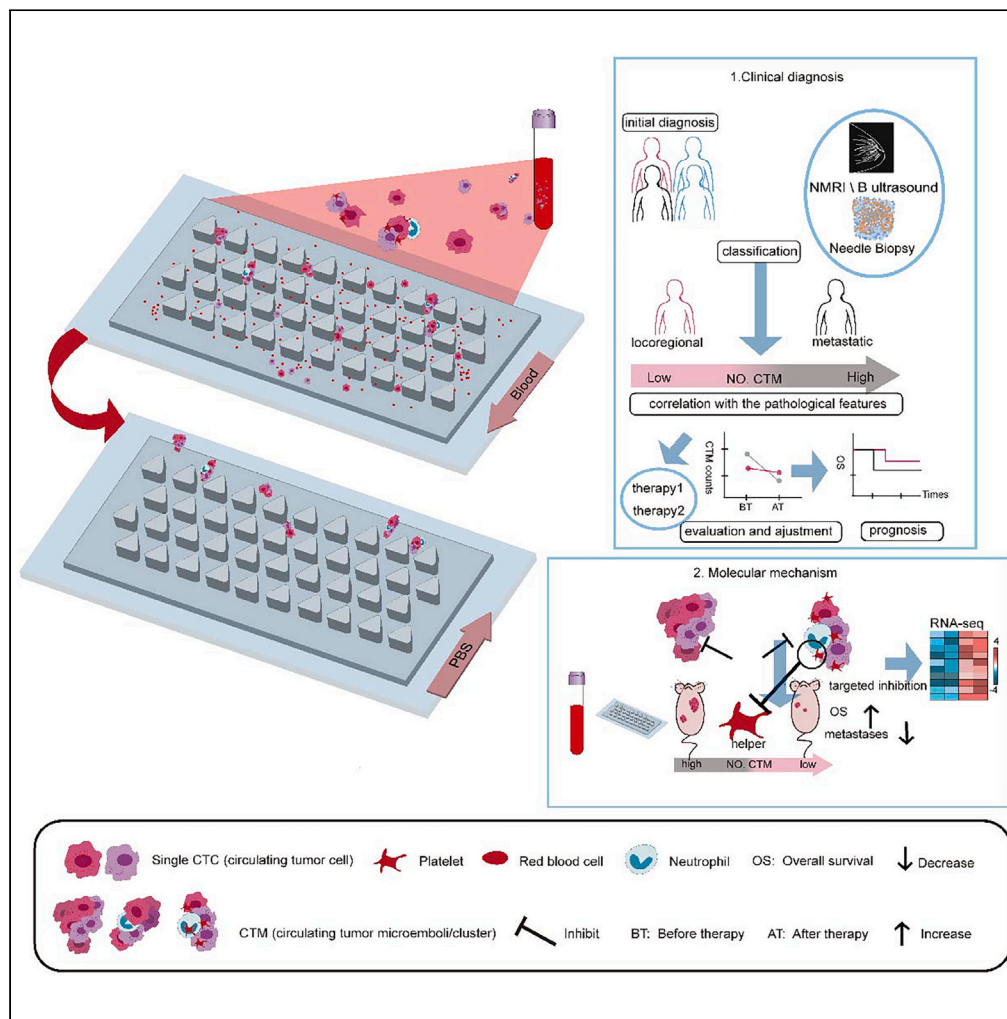


Article

Hypoxia stimulates CTC-platelet cluster formation to promote breast cancer metastasis



Weijia Zhou,
Chengjun Zhu,
Peiliang Shen, ...,
Yanni Song, Xin
Han, Xiaoxiang
Guan

yangfangnju@hotmail.com
(F.Y.)
1525@hrbmu.edu.cn (Y.S.)
xhan0220@njucm.edu.cn (X.H.)
xguan@njmu.edu.cn (X.G.)

Highlights
The Cluster-Chip exhibited
easy operation and high
efficiency in isolating CTMs
from clinical samples

Platelet inhibition led to
reduced CTM formation
and facilitation of tumor
metastasis

Hypoxia stimulation and
platelet activation may
correlate to CTC-platelet
cluster formation

Zhou et al., iScience 27, 109547
May 17, 2024 © 2024 The
Authors. Published by Elsevier
Inc.
[https://doi.org/10.1016/
j.isci.2024.109547](https://doi.org/10.1016/j.isci.2024.109547)



Article

Hypoxia stimulates CTC-platelet cluster formation to promote breast cancer metastasis

Weijia Zhou,^{1,7} Chengjun Zhu,^{2,7} Peiliang Shen,^{1,7} Jacqueline F. Wang,^{3,7} Gaoshuang Zhu,¹ Yuanyuan Jia,¹ Yueyao Wu,¹ Siliang Wang,⁴ Jia Sun,¹ Fang Yang,^{5,*} Yanni Song,^{6,*} Xin Han,^{1,*} and Xiaoxiang Guan^{2,8,*}

SUMMARY

Circulating tumor cell clusters/micro-emboli (CTM) possess greater metastatic capacity and survival advantage compared to individual circulating tumor cell (CTC). However, the formation of CTM subtypes and their role in tumor metastasis remain unclear. In this study, we used a microfluidic Cluster-Chip with easy operation and high efficiency to isolate CTM from peripheral blood, which confirmed their correlation with clinicopathological features and identified the critical role of CTC-platelet clusters in breast cancer metastasis. The correlation between platelets and CTM function was further confirmed in a mouse model and RNA sequencing of CTM identified high-expressed genes related to hypoxia stimulation and platelet activation which possibly suggested the correlation of hypoxia and CTC-platelet cluster formation. In conclusion, we successfully developed the Cluster-Chip platform to realize the clinical capture of CTMs and analyze the biological properties of CTC-platelet clusters, which could benefit the design of potential treatment regimens to prevent CTM-mediated metastasis and tumor malignant progression.

INTRODUCTION

Circulating tumor cells (CTCs) are tumor cells that shed from a primary tumor site, subsequently enter the circulatory system, and can further extravasate, colonize, and grow to form metastases due to their unique and complex phenotypic and genetic characteristics.^{1,2} Thus, cancer metastasis is closely related to the dissemination of CTCs. The isolation of CTCs from the circulatory system not only represents a breakthrough in the examination of the phenotypic and genetic characteristics of primary tumors, but also facilitates further understanding of the mechanisms underlying hematogenous metastasis.³ The detection of CTCs is not routinely used in clinical practice, but they could be important in the diagnosis, clinical staging, drug efficacy evaluation, and prognostic assessment of tumors as biological properties are revealed.^{4,5}

CTCs exist as single or multicellular aggregates known as circulating tumor cell clusters/micro-emboli (CTM) depending on their interactions with other cells in the circulation.^{6,7} The molecular mechanisms involved in the formation of CTM remain largely unknown.⁸ Prior studies have demonstrated that CTM that were isolated from the primary tumor in the form of clusters may originate from the intravascular aggregation of individual CTCs.⁹ Later studies reported that CTM exhibited greater metastatic capacity and survival advantage over individual CTCs.^{10,11} Studies using mouse models confirmed the greater metastatic capacity of CTM compared with individual CTCs, with findings demonstrating that injecting aggregated clusters of cancer cells resulted in markedly increased tumor formation when compared to injecting the same number of individual cancer cells into mice.^{12,13} Researchers have found that multicellular CTM can be divided into homogeneous CTM and heterogeneous CTM with different mechanisms of formation and function. Compared with single CTCs, homogeneous CTM exhibited more plastic and stem-like properties with features including high expression of adhesion molecules, tight junction proteins, DNA methylation levels, and the process of epithelial-mesenchymal transition (EMT).¹⁴ Heterotypic CTM are not only the aggregation of single cancer cells, but also include many supporting cells such as erythrocytes, fibroblasts, and immune cells that assist in the metastatic survival of CTM.^{15,16} In addition, aggregation with platelets may protect tumor cells from immune surveillance and fluid shear¹⁷; however, the mechanisms of cluster formation and cell-to-cell interaction remain elusive.

CTM that are enriched with platelets have been shown to confer enhanced survival and metastatic advantages compared to individual CTCs and hold immense promise as target entities for various clinical interventions aimed at improving patient outcomes.¹⁸ There is

¹Jiangsu Collaborative Innovation Center of Chinese Medicinal Resources Industrialization, School of Medicine & Holistic Integrative Medicine, The Second Affiliated Hospital of Nanjing University of Chinese Medicine, Nanjing University of Chinese Medicine, Nanjing 210023, China

²Department of Oncology, The First Affiliated Hospital of Nanjing Medical University, Nanjing 210029, China

³Department of Medicine, NYU Langone Health, 550 First Avenue, New York, NY 10016, USA

⁴Department of Pharmacy, Nanjing Drum Tower Hospital, The Affiliated Hospital of Nanjing University Medical School, Nanjing 210008, China

⁵The Comprehensive cancer Center of Nanjing Drum Tower Hospital, Affiliated Hospital of Medical School, Nanjing University, Nanjing 210008, China

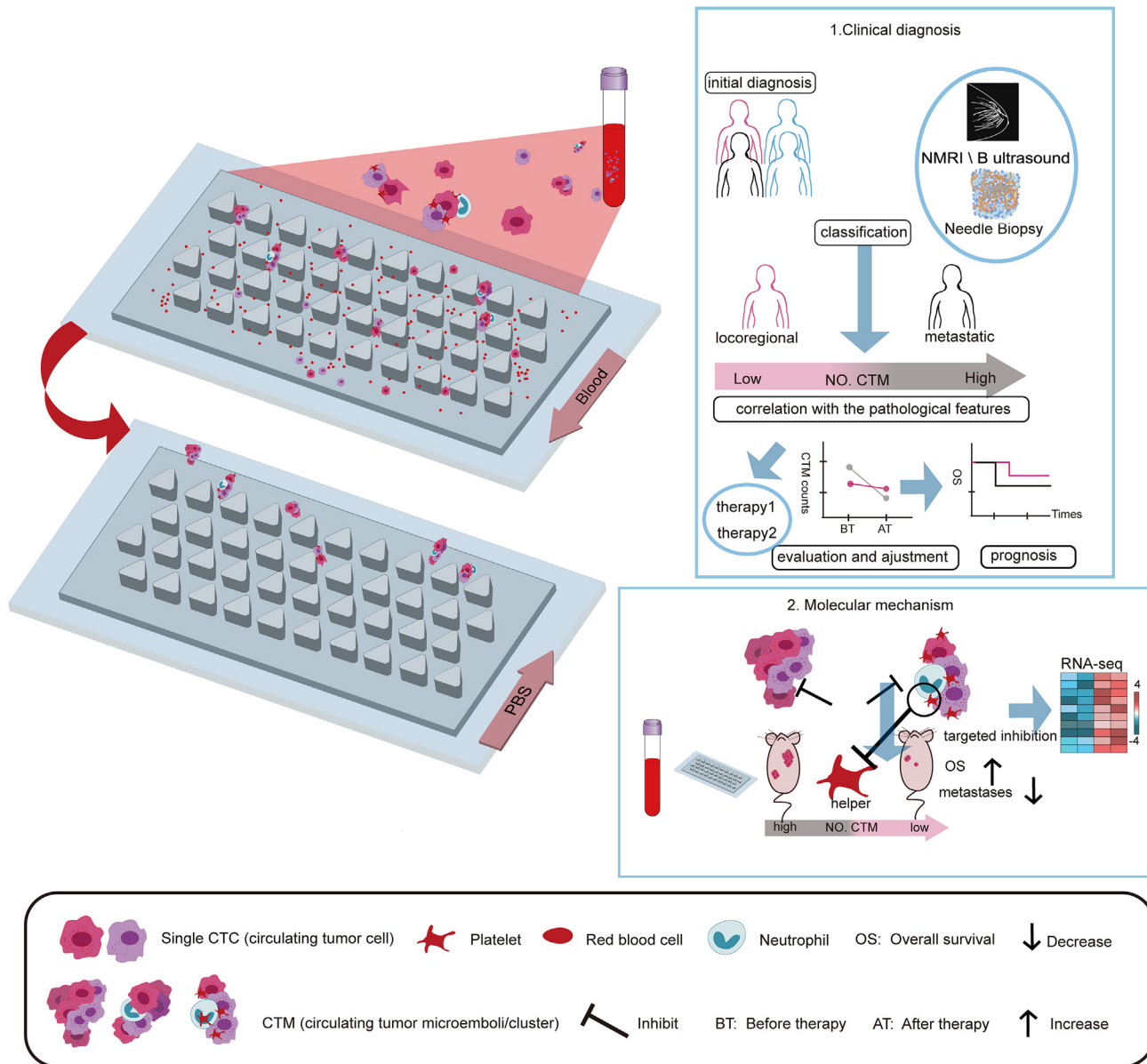
⁶Department of Breast Surgery, Harbin Medical University Cancer Hospital, 150 Haping Road, Harbin 150081, China

⁷These authors contributed equally

⁸Lead contact

*Correspondence: yangfangnju@hotmail.com (F.Y.), 1525@hrbmu.edu.cn (Y.S.), xhan0220@njucm.edu.cn (X.H.), xguan@njmu.edu.cn (X.G.)
<https://doi.org/10.1016/j.isci.2024.109547>





Scheme 1. Schematic diagram of the Cluster-Chip developed for CTM isolation

Schematic diagram of the Cluster-Chip developed for CTM isolation. Sequential validation of the clinical applicability of the Cluster-Chip and mechanism of circulating tumor cell micro-embolus (CTM) in breast cancer metastasis.

a great need for effective and specific CTM isolation techniques to better clarify the mechanisms underlying the function of different CTM subtypes in tumor metastasis. Microfluidic chip technology possesses obvious advantages in its ability to isolate unique cell populations in a rapid and efficient manner.^{19,20} Therefore, this study aimed to develop a microfluidic Cluster-Chip with the ability to specifically capture CTM from peripheral blood for evaluation with clinical samples and validation for clinicopathological applicability. Moreover, the biological properties of CTM and its potential mechanisms in tumor metastasis were investigated by successful CTM isolation in a mouse model. The critical role of the CTC-platelet cluster was identified by findings suggesting that platelet inhibition was shown to result in reduced CTM formation and tumor metastasis. RNA sequencing (RNA-seq) analysis and following verification experiments possibly suggested that hypoxia played an important role in CTC-platelet cluster formation and tumor malignant progression, which may provide a promising clinical target in tumor therapy. A schematic diagram demonstrating the clinical applicability of the Cluster-Chip in CTM isolation and the mechanism of CTM in breast cancer metastasis is outlined in [Scheme 1](#).

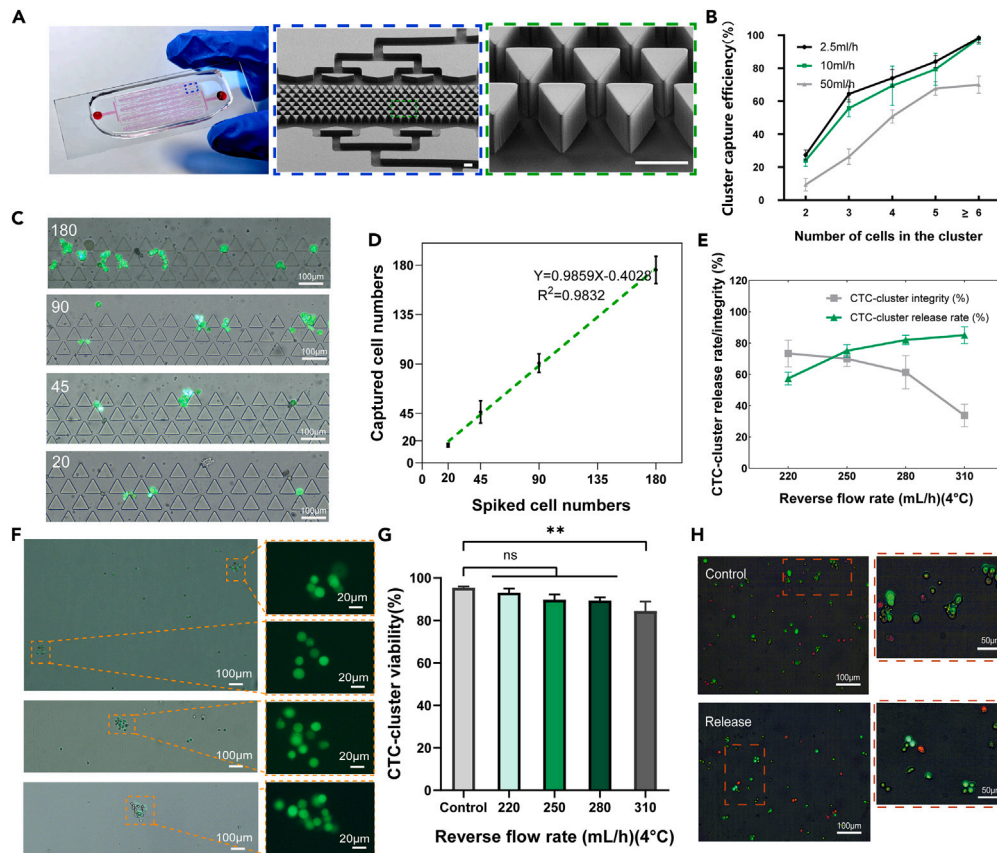


Figure 1. Performance and optimization experiments for determining capture and release efficiency

(A) Diagram of the overall and internal structure of the Cluster-Chip. Scale bar: 100 μm .

(B) Capture efficiency at different flow rates measured at 4°C. The Cluster-Chip was filled with Pluronic F127 (1% w/v in PBS) to minimize cell adhesion using artificial clusters of A549 cells spiked in whole blood.

(C and D) 4T1 cells that were stained by CFSE ranged from 20, 45, 90, and 180 in total number and were spiked into 1 mL of healthy blood. Fluorescent images of the captured cell clusters on the chip are shown. Scale bar: 100 μm (C). Captured vs. input cell number (D).

(E) Release efficiency and integrity of cell clusters from the chip as a function of the reverse flow rate at 4°C.

(F) Images of the intact cell clusters captured following release into the solution from the Cluster-Chip operated at 250 mL/h. Scale bar: 100 μm and 20 μm .

(G) Percentage of viable cell clusters released at different flow rates using Cluster-Chip against the control group.

(H) Fluorescent images of cell clusters treated with two-color viability (green)/cytotoxicity (red) assay. The cells are divided in two batches including control and cell clusters captured and released from Cluster-Chip at 250 mL/h. Scale bar: 100 μm and 50 μm . Data were presented as mean \pm SD. ** $p < 0.01$.

RESULTS

Chip optimization and performance

The structure of the Cluster-Chip was based on the separation principle of physical properties such as cell size, which was developed according to a previously published device with simpler structure of reducing capture traps.²¹ Details regarding internal structure and parameters are shown in Figures 1A and S1. In order to achieve better isolation performance, artificial carboxyfluorescein succinimidy ester (CFSE)-labeled cell-clusters/CTM was spiked with phosphate-buffered saline (PBS) or healthy whole blood to screen for a suitable captured flow rate. Through repeating the experiments at different flow rates, the Cluster-Chip yielded more than 90% of capture efficiency for larger clusters under slightly lower rates, which avoided breaking up the captured CTM and ensured a certain capture for small-sized CTM (Figure 1B). We considered the efficient isolation and timeliness for the captured process and chose 10 mL/h as the optimal flow rate. Figures S2A and S2B exhibits the artificial CTM trapped on the Cluster-Chip. The chip consists of four large row traps which contained seven small rows with three consecutive triangular column-like traps. We recorded the distribution of the cell-clusters on the four rows to verify the successful capture indirectly (Figure S2B). To ensure that the cell clusters were not damaged compared with those before separation, cells with different density were seeded into the ultra-low attachment well plates for forming clusters following capture and release (Figure S2C). We found that after capturing, our chip not only preserved the almost equivalent quantities of spiked cell clusters, but also intuitively relied on cluster size, including how many numbers of single cells were needed to recognize and classify efficiently (Figure S2D). In order to further simulate the blood environment and eliminate the effect of blood cells on the capture efficiency of the chip, we spiked a certain number of CFSE-labeled

CTM into the whole blood of healthy animals for chip processing. The accuracy of capture was similar to when spiking in PBS (Figures 1C and 1D). As is widely recognized, it is necessary to release captured CTM from pathological whole blood to ensure their effective recovery for further evaluation. Therefore, it is the first step in exploring optimal flow rates for the release of CTM to facilitate their efficient retrieval. On the premise of not damaging viability and morphology, we conducted recovery experiments with different flow rates. The integrity and release rate of CTM showed the opposite trend with an increase of the rate. Thus, we selected the flow rate of 250 mL/h for recovery (Figure 1E), which was able to maintain high integrity (Figure 1F) and viability (Figures 1G and 1H).

Evaluation of CTM from breast cancer patients using the Cluster-Chip

To assess the potential clinical application of the chip, we applied the Cluster-Chip to isolated CTM from blood samples of breast cancer (BC) patients. Detailed experimental procedure and clinical information of the BC patients are displayed in Table S1 of supplementary data. Following the isolation, we fixed the captured cells on the chip with 4% paraformaldehyde (PFA) and then immuno-stained with specific disease marker pan-CK, leukocyte marker CD45R or platelet marker P-selectin, and nuclear stain 4,6-diamidino-2-phenylindole (DAPI) as the confirmed reagents. Homogenous CTM were marked as pan-CK+/CD45R-/DAPI+ or pan-CK+/P-selectin-/DAPI+ and heterogenous CTM were identified as pan-CK+/CD45R+/DAPI+ or pan-CK+/P-selectin+/DAPI+, demonstrated in Figures 2A, 2B, and S3A. CTM were more metastatic but rarer than single CTCs; thus, exploring the characterization of the CTM is urge for thoroughly understanding the mechanism of metastasis. The correlation between the enumeration of single CTCs and clinical pathological features were confirmed by several reports over the past few years.^{22,23} Some conventional serum markers were linked with the CTC counts detected in patients,^{24,25} which suggest that CTCs can be used as potential breakthroughs to solve the present cancer metastasis dilemma. However, CTM consisting of a clustering type of single CTCs with or without other non-tumor cells can be regarded as more malignant CTCs.⁷ Therefore, the CTM counts were enumerated and linked with clinical indicators in our study (Table S2). As commonly reported, metastasis is one of the primary reasons for death in tumor patients. Our results also found that patients with disease without metastasis had fewer CTM counts than those with metastasis in lymph nodes or distant metastasis, suggesting that CTM counts could be a valuable tool to monitor metastatic progression (Figures 2C and 2D). We also focused on the level of markers commonly used to assist in the diagnosis of breast cancers such as Carcinoembryonic antigen (CEA), CA125, and CA153. Prior studies have combined these traditional diagnosis indexes with single CTC counts in peripheral blood of cancer patients to provide more effective and accuracy diagnosis performance. We aimed to determine if there are similar interactions between CTM and these indexes (Table S3). In our study, we found that CTM count showed no significant correlation with CA125 and CA153 levels; however, CEA levels exhibited a significant correlation with CTM counts (Figures 2E, S3B, and S3C). As this may be due to our limited clinical samples, more samples should be tested to acquire more wide and meaningful data.

To evaluate the occurrence of distinct CTM types in patients, we categorized them into two groups: those with distant metastasis and those with locoregional disease, which comprised patients either with only primary tumors or with adjacent lymph node metastases. Overall, CTM were detected in a majority of patients with a detection rate of 95% and 66.7% in the distant metastasis and locoregional groups, respectively. Notably, both groups exhibited a high proportion of heterogeneous CTM, with 70% of CTM being heterogeneous in the distant metastasis group, and 50% in the locoregional group. (Figure 2F). Heterogenous CTM included non-malignant counterparts that were believed to provide advantages for CTM survival and effective metastases. The other cell components were identified by multiple immuno-stains with 8 identified in distant metastasis and 5 in locoregional groups. As seen in Figure 2G, the most common CTM comprised CTC-CTC clusters followed by CTC-platelet clusters, with detailed counts illustrated in Figure 2H.

Evaluation of the effect of platelet intervention on metastasis by Cluster-Chip

Clinical studies have confirmed that cancer patients with high-risk thrombosis often have poor prognosis, implicating the involvement of platelets in cancer progression. Platelets thus act as so-called "allies" of tumor growth and metastasis and are believed to resist cell death, promote EMT, facilitate immune system escape, and encourage extravasation.^{26,27} Notably, aforementioned clinically isolated samples also contained heterogeneous CTM composed of platelets.

To reveal the key role of platelets in the formation of CTM, an experimental model of breast cancer metastasis was constructed in female BALB/c mice through tail-vein injection of 4T1-Luc cells and two kinds of drugs that have the opposite effects on platelets with aspirin (ASA) and U46619 supplemented respectively. *In vivo* bioluminescence imaging (BLI) evaluated the formation of lung metastases in mice in different treatment groups. To avoid the differences of initial injections, we performed the tail-vein injection of the same number of 4T1-Luc cells in each group with repeat experiments. Whole blood from mice in each group was collected and isolated by the Cluster-Chip once metastasis occurred at a suitable time. As shown in Figures 3A and 3B, the BLI intensities of the lungs from mice that were treated with ASA showed fewer metastatic lung nodules; however, there were no significant differences in lung bioluminescence signals among the other three groups. One reasonable explanation was that U46619 may cause excessive activation of platelets in a normal hemostasis system, causing blood to flow slowly and thus leading to little metastasis. In addition, pharmacological effects of the combined administration group could be neutralized, which generated metastasis close to that of the control mice. Consistent with the aforementioned results, it was clear that when platelets were impaired by ASA and restored by U46619, the platelet activation group and the combination treatment group were able to capture more CTM than the inhibition groups. Among the inhibition groups, the ASA treatment group captured the least number of CTM, originally suggesting that activated platelets indeed play an important role on metastasis (Figures 3C and 3D). Moreover, H&E staining of the mouse lungs confirmed the lower incidence of metastases here (Figure 3E) and fewer metastatic lung nodules in the mice treated with ASA (Figure 3F).

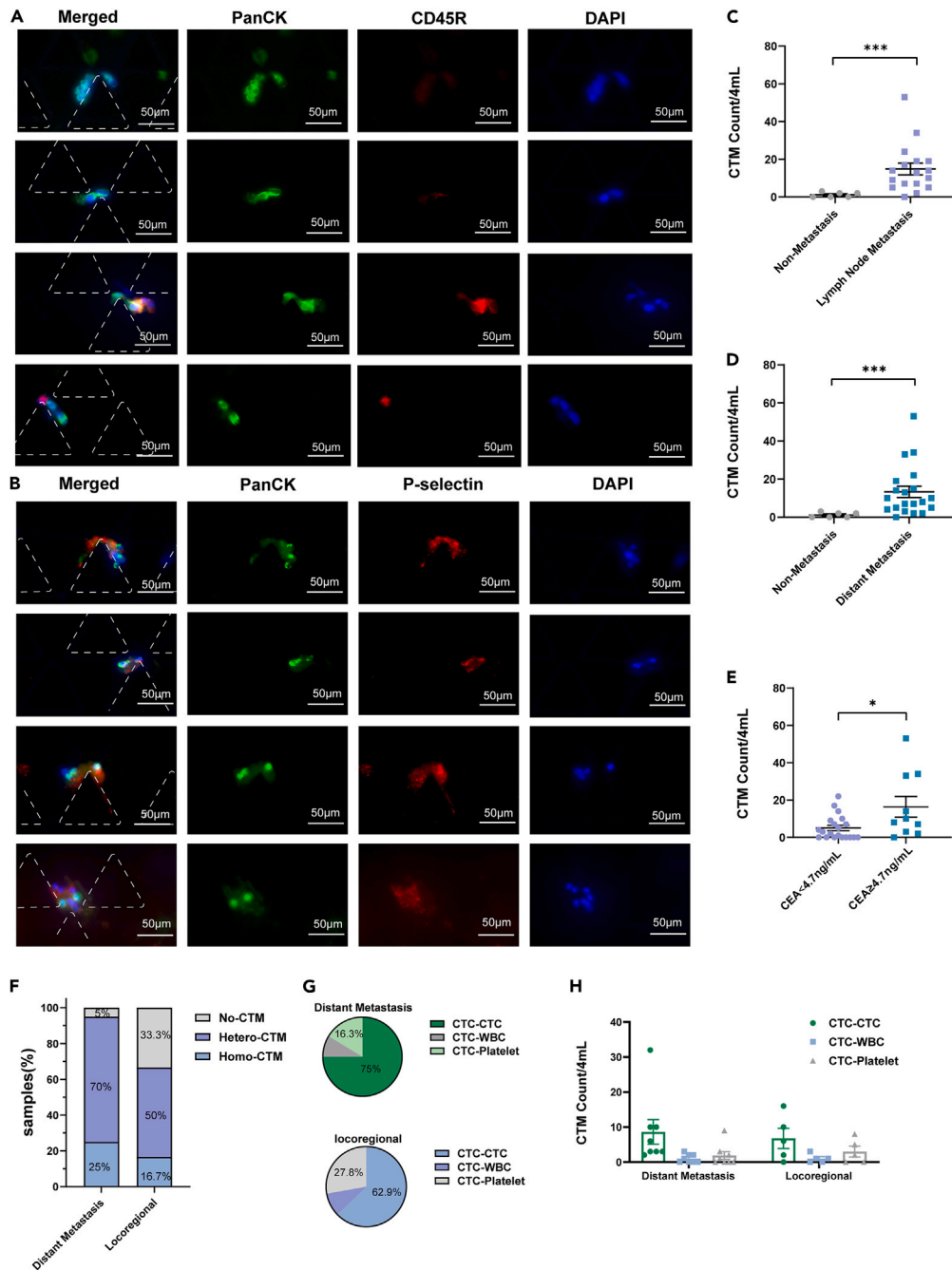


Figure 2. Characterization and enumeration of CTM isolated from blood samples from breast cancer patients

(A and B) Representative fluorescent micrographs of homotypic and heterotypic CTM in different sizes including neutrophils or platelets, respectively. Captured cells were stained with Cytokeratin (green), CD45 or P-selectin (red), DAPI (nuclei, blue). Scale bar: 50 μ m.

(C and D) CTM counts per 4 mL of peripheral blood samples from BC patients with non-metastasis ($n = 6$), lymph node metastasis ($n = 17$), and distant metastasis ($n = 20$).

(E) CTM counts of BC patients with CEA <4.7 ng/mL and CEA ≥ 4.7 ng/mL.

(F) Percentages of BC patients with different detectable types of CTM in distant metastasis ($n = 20$) and locoregional BC patients ($n = 12$).

(G) Various CTM percentages from distant metastasis ($n = 8$) and locoregional BC patients ($n = 5$).

(H) CTM counts for patients with different disease states across different types of CTM, corresponding to (G). Data are represented as mean \pm SEM. $*0.01 < p \leq 0.05$; $***p \leq 0.001$.

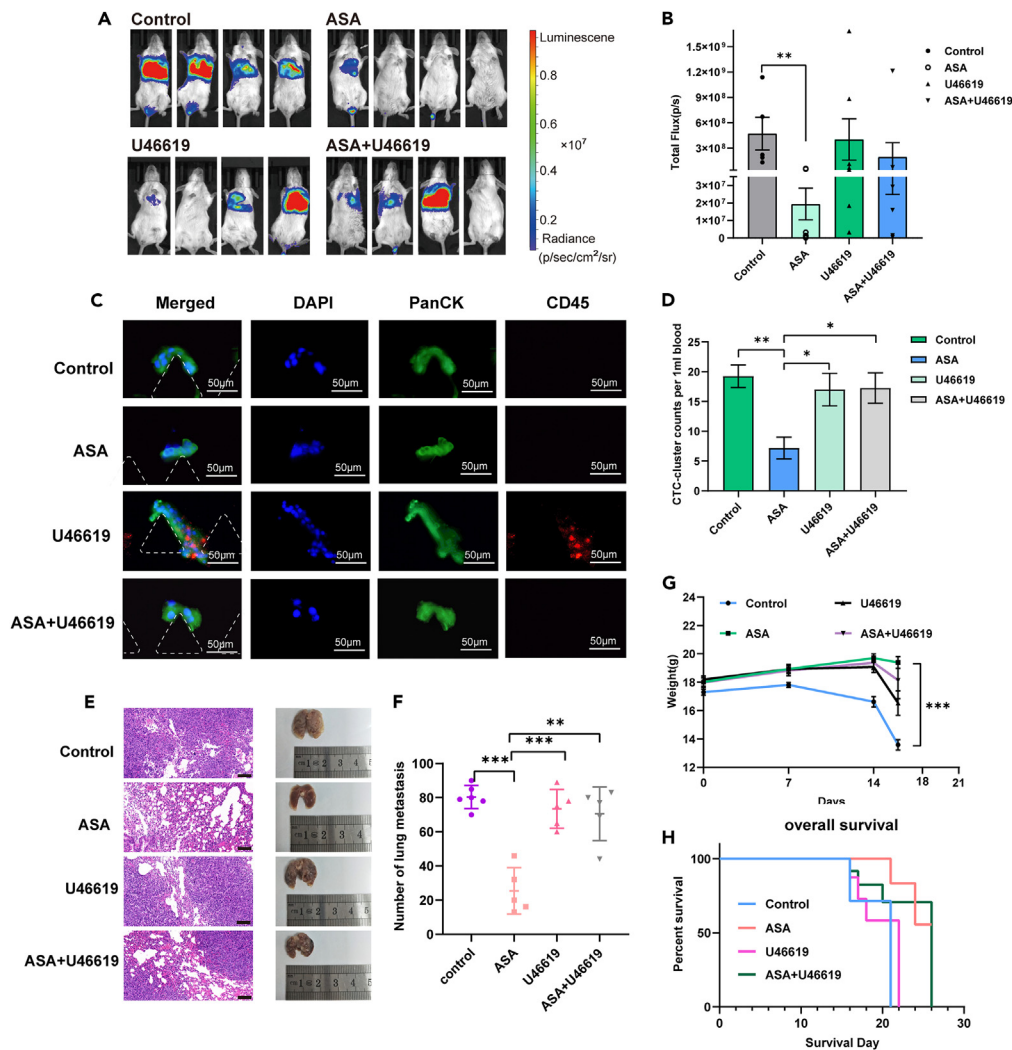


Figure 3. Disturbing the interaction between platelets and CTM led to fewer metastases

(A) IVIS images demonstrating metastasis of 4T1-Luc cells in lungs at the 16th day after injection. BALB/c female mice divided into 4 groups were injected with 1×10^6 cells from the tail vein. Two days prior to 4T1-Luc cell injection, mice were treated with vehicle, aspirin (ASA), U46619, and ASA plus U46619 for 3 weeks ($n = 7, 9, 8,$ and $8,$ respectively).

(B) The total flux of the cells in the mice in different groups.

(C) Representative images of CTC clusters isolated from mice with metastatic breast cancer to the lungs. CTC clusters were stained with Pan-cytokeratin (green), CD45 (red), and DAPI (nuclei, blue). Scale bar: $50 \mu\text{m}$.

(D) Quantitation of CTC clusters per 1 mL of blood in mice of the 4 groups.

(E and F) H&E staining of lung sections (left) and physical images of the lung (right) (E) The number of mouse lung metastases in different groups (F). Scale bar: $100 \mu\text{m}$.

(G) Change in body weight of mice.

(H) Overall survival curves of the 4 groups of mice. Data are represented as mean \pm SEM. $*0.01 < p \leq 0.05$; $**0.001 < p \leq 0.01$; $***p \leq 0.001$.

Weight change and overall survival of these mice were recorded at set intervals, emphasizing that interference of metastasis can effectively reduce the incidence of mortality to a certain extent (Figures 3G and 3H).

Breast cancer CTM-correlated gene sets are enriched for hypoxia stimulation and platelet activation

Our findings have demonstrated that platelets can affect CTM hematogenous metastasis. In order to further understand the mechanism of CTM hematogenous metastasis, examination of the molecular characteristics of CTM using the Cluster-Chip to isolate viable CTM for downstream molecular assays can aid in elucidating the mechanism of CTM-mediated hematogenous metastasis. For this purpose, we used the Cluster-Chip to recover CTM in mice with lung metastasis secondary to breast cancer for RNA sequencing to investigate the biological

characteristics of hematogenous metastasis. We used the epithelial cell adhesion molecule (EPCAM) and the CD45 antibody to stain live CTM captured and released from 5 mice as one group alongside a control group comprised 3 samples of the 4T1 cell line in a low adherence culture (Figure 4A). In both the experimental and control groups, 1,953 significantly differentially expressed genes were enriched, of which 750 genes were significantly upregulated and 1,203 genes were significantly downregulated in the CTM group, as detailed in Figure S4. Analysis of transcripts corresponding to a selected set of specific feature genes is shown in Figure 4B. The two groups overexpressed different tumor cell-specific keratins (KRT16, KRT19, KRT18, and KRT7) and EPCAM was greatly differentially expressed in the experimental groups but lowly expressed in all control groups. The vast majority of genes related to mesenchymal state and stemness were highly expressed in the CTM group, revealing the existence of a mixed EMT state characteristic of *in vivo* CTM.^{28,29} Thus, it was shown that cell aggregation allowed interaction between cells of different epithelial mesenchymal states, which can enhance their potential for colonization at distant sites.^{30,31} Leukocyte-associated genes, namely macrophage-derived CD68, OIT3, and monocyte-derived CD33, were also detected in the CTM group in addition to platelet-associated genes detected in CTM, which confirmed the presence of heterogeneous CTM, or aggregates of tumor cells and non-tumor cells.

As seen in Figure 4C, Gene Ontology enrichment analysis demonstrated that differently expressed genes were mainly enriched in response to oxygen levels, hypoxia, and decreased oxygen levels. The expression of genes associated with mediating CTM metastasis and thus malignant progression of the tumor was also screened (Figure 4D). Interestingly, the genes marked as red were all related to hypoxic stimulation. Hypoxia-inducible factor (HIF)-mediated signaling in malignant cells influences multiple steps in the metastatic process including invasion and migration, endocytosis and exocytosis, establishment of pre-metastatic microhabitats, and survival and growth at distant sites.³² As seen in the Kyoto Encyclopedia of Genes and Genomes (KEGG) enrichment bubble plots in Figure S5, the HIF-1 signaling pathway was significantly altered in the CTM compared with the control group (Q-value < 0.01). Gene Set Enrichment Analysis (GSEA) showed that the HIF-1 signaling pathway genes in the CTM were positively enriched in the experimental group (Figure S6). In addition, the genes labeled with green were associated with platelet activation, indicating that platelets also play an important role in CTM-mediated metastasis. All of these genes were differently expressed in the CTM group, reinforcing the stronger malignant potential of CTM.

We further focused on the association between genes and stimulation of hypoxia through examining the genes ENO2 and ENO3, which encode enolase, a key enzyme of the glycolytic pathway. The gene encoding the inducible enzyme nitric oxide synthase, NOS2, has been implicated in the processes of wound healing, angiogenesis, and carcinogenesis in many studies. In addition, the vascular endothelial growth factor A (VEGFA) and serpin family E member 1 (SERPINE1) genes both play important roles in tumor angiogenesis.^{33,34} The adrenomedullin (ADM) gene encodes the pro-angiogenic factor ADM, which is differentially expressed in CTM and control groups, as shown in the volcano plot in Figure S7. Tumor cell-derived ADM has pro-angiogenic and direct pro-tumor effects.³⁵ ENO2, ENO3, NOS2, and ADM genes were also enriched in the top 20 most significantly upregulated and downregulated genes in CTM vs. control group (Figure S8). Given the relationship between platelets and CTM *in vivo*, there was special attention to genes related to platelet activation such as the integrin subunit alpha 2b (ITGA2b) gene that encodes platelet protein CD41, whose expression is essential for platelet aggregation.³⁶ In addition, the chitinase 3 like 1 (CHI3L1) gene plays a key role in hepatic platelet recruitment during acetaminophen-induced liver injury and studies have shown that CHI3L1 protein secreted by tumor-associated macrophages promotes metastasis in gastric and breast cancers.³⁷ Furthermore, the G protein-coupled receptor 35 (GPR35) gene promotes rapid recruitment of neutrophils to sites of inflammation, with function in neutrophil recruitment strongly dependent on platelets.³⁸ GPR35 pathway activation is able to drive angiogenesis in the tumor microenvironment and its high expression in tumor tissues is closely associated with poor prognosis.³⁹ In this study, these genes were verified by qPCR (Figure 4E) and the relationship between these genes and overall survival of BC patients were subsequently analyzed with Kaplan-Meier curves (Figure S9). RNA sequencing results demonstrated that genes associated with hypoxia stimulation and platelet activation were both upregulated. Prior studies have reported that a hypoxic environment can induce aggregated tumor cell metastasis.^{40,41} Moreover, hypoxic environments can activate platelets, which can then contribute to hypoxia-induced inflammation to a certain extent.^{42,43} Meanwhile, given the fact that platelets commonly assist in tumor bloodstream metastasis, we speculated that hypoxic environments stimulate platelet activation and are thus beneficial to tumor cell adhesion and platelet aggregation in the formation of additional CTC-platelet clusters. Therefore, we designed an *in vitro* hypoxic tumor cell-platelet adhesion and aggregation assay, followed by Cluster-Chip capture for counting and quantification. When tumor cells and platelets were co-cultured in low adherence plates, the group under hypoxic conditions was able to form more heterotypic CTC-platelet clusters than in a normoxic conditions, accounting for 80% of the total clusters (>4) in this group (Figures 4F and 4G). This may be useful in comprehending the upregulation of gene expression associated with platelet activation and hypoxia stimulation in the CTM group. Thus, our results originally suggested that that tumor cells adhered to more platelets in hypoxic conditions and subsequently formed heterotypic CTC-platelet clusters that ultimately possibly promoted tumor metastasis.

DISCUSSION

In this study, the microfluidic Cluster-Chip was constructed with the specific purpose of separating CTM based on the principle of cell size separation. To simulate peripheral blood capture more realistically, a known number of simulated cell clusters were added to the peripheral blood of healthy mice and both separated and recovered using the screened rate. The results were consistent in indicating that the Cluster-Chip can be used for subsequent peripheral blood isolation experiments due to its ability to specifically isolate CTM in a simple and efficient manner. Peripheral blood samples were isolated from 32 BC patients using Cluster-Chip and homotypic CTM consisting of multiple tumor cell aggregates and heterotypic CTM containing tumor and non-tumor cells, platelets, or leukocytes were detected by immunofluorescence, confirming the clinical applicability of the Cluster-Chip. Clinical information and statistical analysis revealed the correlation between the presence

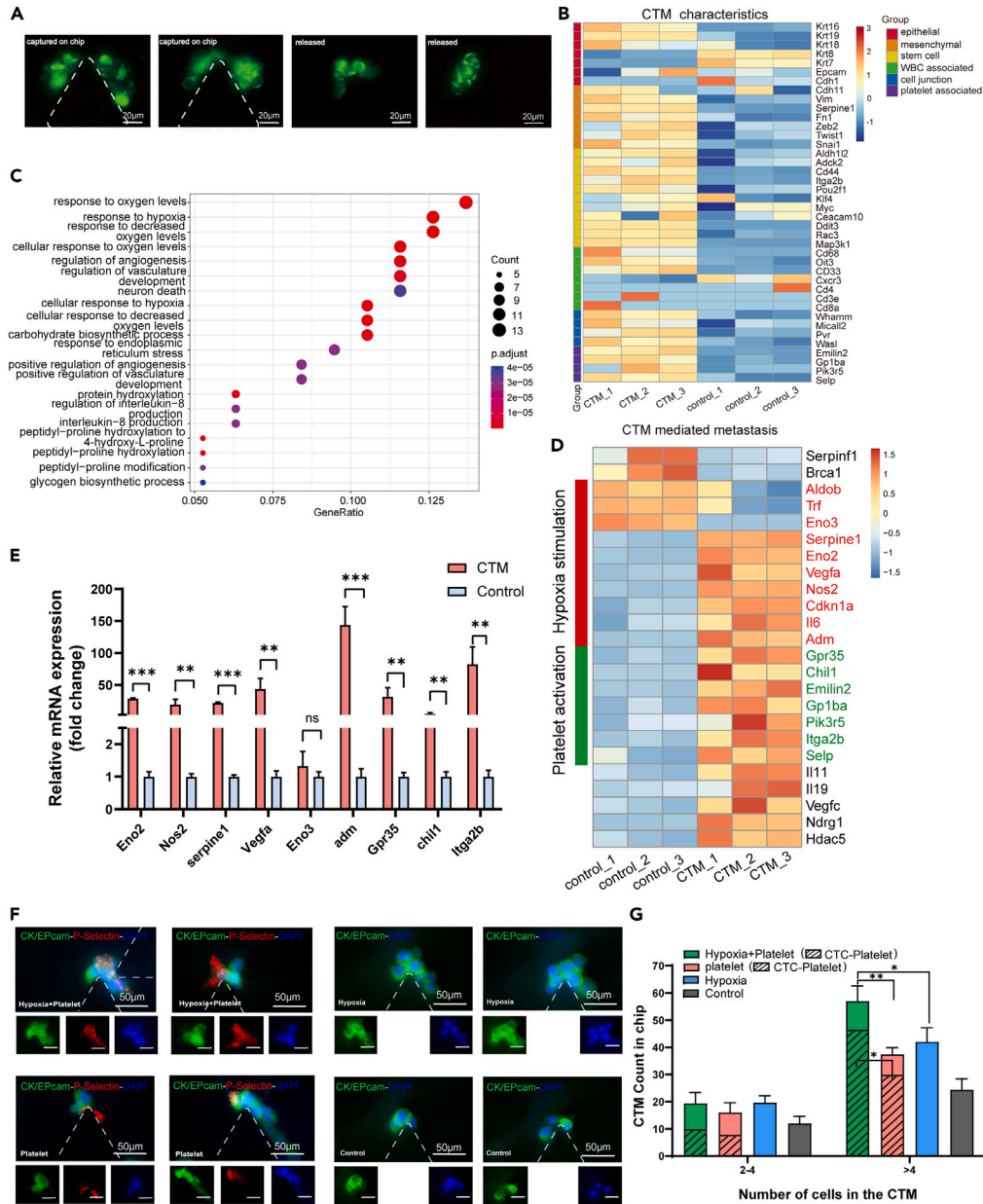


Figure 4. Specific genes related to hypoxia stimulation and platelet activation were enriched in the CTM group versus the control group

(A) Images of CTM released from the Cluster-Chip and live stained with FITC anti-mouse CD326 (EPCAM) (green) and Alex594-conjugated antibodies against CD45 (red).

(B) Heatmap of gene expression related to epithelial status, mesenchymal status, cell stemness, leukocytes, cell junctions, and platelets in samples from each group.

(C) Gene Ontology enrichment analysis in treatment vs. control groups.

(D) Heatmap of gene expression associated with CTM-mediated metastasis in the two groups of samples, with some genes marked with red and some marked with green relating to hypoxia stimulation and platelet activation, respectively.

(E) Verification of key genes that are differently expressed in treatment vs. control group by qPCR.

(F) Representative fluorescent micrographs of 4T1 cell clusters captured on the chip following culture in ultra-low adhesion well plates with or without platelets under the hypoxic or normoxic conditions. CTC-clusters stained for Pan-cytokeratin and EPCAM (green), P-selectin (red), and DAPI (nuclei, blue). Scale bar: 50 μ m and 20 μ m.

(G) The statistic quantification of the different types of captured CTM cultured in 4 conditions as mentioned in (F). Data were presented as mean \pm SD. * $0.01 < p \leq 0.05$; ** $0.001 < p \leq 0.01$; *** $p \leq 0.001$.

of CTM and certain clinicopathological features, emphasizing the important role of CTM in breast cancer metastasis. Notably, a study of head and neck cancer utilized microfluidic microarray structures to capture CTM in patient blood samples. They demonstrated that CTC clusters contained Epidermal growth factor receptor (EGFR) amplified single CTCs within the cluster volume and also emphasized the important biological roles of these cell populations in tumor metastasis.⁴⁴

With increased platelet counts being a risk factor for metastasis in cancer patients,⁴⁵ we also explored the association between platelets and CTM by intervening with platelets to assess the impact of platelets on cancer metastasis from the perspective of changes in CTM counts. Platelets were treated with platelet inhibition, activation, and inhibition followed by activation in mice with lung metastasis from breast cancer, with occurrence of metastasis monitored via *in vivo* imaging. The results confirmed that there was a correlation between platelets and the *in vivo* level of CTM, and that platelet inhibition led to a decrease in CTM formation and thus affected metastasis. To further investigate the mechanism of CTM-mediated hematopoietic metastasis, the Cluster-Chip was used to capture and recover CTM from breast cancer lung metastasis *in vivo* in mice. RNA sequencing was executed to investigate the biological characteristics of hematopoietic metastasis. High expression of genes in mediating CTM metastasis by hypoxia stimulation and platelet activation were identified in the CTM group. These genes can potentially be used for targeting CTM to restrict cancer metastasis in future studies. However, studies on these genes in the field of cancer are still complex and diverse, and further research is necessary for more definitive conclusions to be drawn.

In conclusion, the Cluster-Chip isolation platform is a powerful tool for clinical cancer detection and laboratory research on metastasis. Fully utilizing the microfluidic platform can not only enable the exploration of the association between CTM and disease progression, but can also provide a deeper understanding of cancer metastasis by analyzing molecular characteristics and lead to the improvement of existing treatment options and the discovery of meaningful therapeutic targets.

Limitations of the study

In the application of clinical samples, the number of isolated patients should be as large as possible and cover the whole range of patients, and the CTM changes should be linked to the various pathological indicators of patients. It is better to track and detect the difference in the number of CTMs in the patient's body during the whole treatment process, and evaluate the efficacy and prognosis of the treatment. At the same time, it is better to continuously optimize the parameters of the chip and upgrade its performance to improve the stability of the platform's separation ability and the accuracy of CTM counting. For the animal model, the tumor metastasis model was constructed in this study via tail vein injection of tumor cells. *In situ* spontaneous metastasis would be better to be constructed subsequently to truly simulate the whole process of cancer metastasis in the clinic setting.

STAR★METHODS

Detailed methods are provided in the online version of this paper and include the following:

- KEY RESOURCES TABLE
- RESOURCE AVAILABILITY
 - Lead contact
 - Materials availability
 - Data and code availability
- EXPERIMENTAL MODEL AND STUDY PARTICIPANT DETAILS
 - Cell culture and preparation
 - Construction of experimental lung metastasis
 - Blood samples preparation
- METHOD DETAILS
 - Chip design and development
 - Device operation
 - Cell-cluster spiking experiments
 - Fluorescent live and dead assays
 - Blood processing and immunofluorescence staining
 - Drug intervention in lung metastases of mice
 - *In vivo* bioluminescence imaging and tumor progression
 - RNA extraction library construction and RNA sequencing
 - Bioinformatics pipeline
 - qPCR reaction
 - Hypoxia experiments
- QUANTIFICATION AND STATISTICAL ANALYSIS

SUPPLEMENTAL INFORMATION

Supplemental information can be found online at <https://doi.org/10.1016/j.isci.2024.109547>.

ACKNOWLEDGMENTS

This study was funded by the National Natural Science Foundation of China (81920108029 and 82002783); the Key Foundation for Social Development Project of the Jiangsu Province of China (BE2021741); the Priority Academic Program Development of Jiangsu Higher Education Institutions (Integration of Chinese and Western Medicine); Jiangsu Key Discipline Construction Fund of the 14th Five-Year Plan (Biology); Ministry of Education Chunhui Project Cooperative Research Project (No. HLJ2019010); Heilongjiang Natural Science Foundation of China (No. LH2020H120); Beijing MDK Public Welfare Foundation Research Fund (No. MDK 2022-1001); Haiyan Fund of Harbin Medical University Cancer Hospital (No. JJZD2020-04); Postdoctoral Scientific Research Developmental Fund of Heilongjiang (No. LBH-Q22); The Graduate Research & Practice Innovation Program of Jiangsu Province (SJCX22_0780, KYCX21_1743, and KYCX22_1987).

AUTHOR CONTRIBUTIONS

X.G., X.H., Y.S., and F.Y. conceived the idea and designed the experiments. W.Z., C.Z., and P.S. performed the majority of experimental work and data analysis. G.Z. and Y.J. assisted chip development and performed cell analysis. Y.W. and J.S. assisted in animal experiments. X.G., S.W., and C.Z. collected the clinic sample for analysis. X.H., J.F.W., and W.Z. wrote the manuscript with feedback from all the authors. All authors have approved the final version of the manuscript.

DECLARATION OF INTERESTS

The authors declare no competing interests.

Received: October 16, 2023

Revised: January 2, 2024

Accepted: March 18, 2024

Published: March 20, 2024

REFERENCES

- Sethi, N., and Kang, Y. (2011). Unravelling the complexity of metastasis - molecular understanding and targeted therapies. *Nat. Rev. Cancer* 11, 735–748.
- Gerstberger, S., Jiang, Q., and Ganesh, K. (2023). Metastasis. *Cell* 186, 1564–1579.
- Pantel, K., and Alix-Panabières, C. (2022). Crucial roles of circulating tumor cells in the metastatic cascade and tumor immune escape: biology and clinical translation. *J. Immunother. Cancer* 10, e005615.
- Ward, M.P., E Kane, L., A Norris, L., Mohamed, B.M., Kelly, T., Bates, M., Clarke, A., Brady, N., Martin, C.M., Brooks, R.D., et al. (2021). Platelets, immune cells and the coagulation cascade; friend or foe of the circulating tumour cell? *Mol. Cancer* 20, 59.
- Krebs, M.G., Metcalf, R.L., Carter, L., Brady, G., Blackhall, F.H., and Dive, C. (2014). Molecular analysis of circulating tumour cells: biology and biomarkers. *Nat. Rev. Clin. Oncol.* 11, 129–144.
- Lin, D., Shen, L., Luo, M., Zhang, K., Li, J., Yang, Q., Zhu, F., Zhou, D., Zheng, S., Chen, Y., and Zhou, J. (2021). Circulating tumor cells: biology and clinical significance. *Signal Transduct. Target. Ther.* 6, 404.
- Tao, J., Zhu, L., Yakoub, M., Reißfelder, C., Loges, S., and Schölch, S. (2022). Cell-Cell Interactions Drive Metastasis of Circulating Tumor Microemboli. *Cancer Res.* 82, 2661–2671.
- Aceto, N. (2020). Bring along your friends: Homotypic and heterotypic circulating tumor cell clustering to accelerate metastasis. *Biomed. J.* 43, 18–23.
- Maddipati, R., and Stanger, B.Z. (2015). Pancreatic Cancer Metastases Harbor Evidence of Polyclonality. *Cancer Discov.* 5, 1086–1097.
- Hou, J.M., Krebs, M.G., Lancashire, L., Sloane, R., Backen, A., Swain, R.K., Priest, L.J.C., Greystoke, A., Zhou, C., Morris, K., et al. (2012). Clinical significance and molecular characteristics of circulating tumor cells and circulating tumor microemboli in patients with small-cell lung cancer. *J. Clin. Oncol.* 30, 525–532.
- Umer, M., Vaidyanathan, R., Nguyen, N.T., and Shiddiky, M.J.A. (2018). Circulating tumor microemboli: Progress in molecular understanding and enrichment technologies. *Biotechnol. Adv.* 36, 1367–1389.
- Watanabe, S. (1954). The metastasizability of tumor cells. *Cancer* 7, 215–223.
- Fidler, I.J. (1973). The relationship of embolic homogeneity, number, size and viability to the incidence of experimental metastasis. *Eur. J. Cancer* 9, 223–227.
- Schuster, E., Taftaf, R., Reduzzi, C., Albert, M.K., Romero-Calvo, I., and Liu, H. (2021). Better together: circulating tumor cell clustering in metastatic cancer. *Trends Cancer* 7, 1020–1032.
- Szczerba, B.M., Castro-Giner, F., Vetter, M., Krol, I., Gkountela, S., Landin, J., Scheidmann, M.C., Donato, C., Scherrer, R., Singer, J., et al. (2019). Neutrophils escort circulating tumour cells to enable cell cycle progression. *Nature* 566, 553–557.
- Pereira-Veiga, T., Schneegans, S., Pantel, K., and Wikman, H. (2022). Circulating tumor cell-blood cell crosstalk: Biology and clinical relevance. *Cell Rep.* 40, 111298.
- Kanikarla-Marie, P., Lam, M., Sorokin, A.V., Overman, M.J., Kopetz, S., and Menter, D.G. (2018). Platelet Metabolism and Other Targeted Drugs; Potential Impact on Immunotherapy. *Front. Oncol.* 8, 107.
- Bates, M., Mohamed, B.M., Ward, M.P., Kelly, T.E., O'Connor, R., Malone, V., Brooks, R., Brooks, D., Selemidis, S., Martin, C., et al. (2023). Circulating tumour cells: The Good, the Bad and the Ugly. *Biochim. Biophys. Acta. Rev. Cancer* 1878, 188863.
- Jarvas, G., and Guttman, A. (2013). Modeling of cell sorting and rare cell capture with microfabricated biodevices. *Trends Biotechnol.* 31, 696–703.
- Shirai, K., Guan, G., Meihui, T., Xiaoling, P., Oka, Y., Takahashi, Y., Bhagat, A.A.S., Yanagida, M., Iwanaga, S., Matsubara, N., et al. (2022). Hybrid double-spiral microfluidic chip for RBC-lysis-free enrichment of rare cells from whole blood. *Lab Chip* 22, 4418–4429.
- Sarioglu, A.F., Aceto, N., Kojic, N., Donaldson, M.C., Zeinali, M., Hamza, B., Engstrom, A., Zhu, H., Sundaresan, T.K., Miyamoto, D.T., et al. (2015). A microfluidic device for label-free, physical capture of circulating tumor cell clusters. *Nat. Methods* 12, 685–691.
- Zhang, X., Lu, X., Gao, W., Wang, Y., Jia, C., and Cong, H. (2021). A label-free microfluidic chip for the highly selective isolation of single and cluster CTCs from breast cancer patients. *Transl. Oncol.* 14, 100959.
- Qi, Y., Sun, Q., Deng, G., Zhang, H., Xu, Y., Li, Y., Huang, S., Li, Y., Ye, Z., Wang, Y., et al. (2021). Identifying circulating glioma cells and their clusters as diagnostic markers by a novel detection platform. *Clin. Transl. Med.* 11, e318.
- Li, Y., Tian, X., Gao, L., Jiang, X., Fu, R., Zhang, T., Ren, T., Hu, P., Wu, Y., Zhao, P., and Yang, D. (2019). Clinical significance of circulating tumor cells and tumor markers in the diagnosis of lung cancer. *Cancer Med.* 8, 3782–3792.
- Chen, X., Wang, X., He, H., Liu, Z., Hu, J.F., and Li, W. (2015). Combination of circulating tumor cells with serum carcinoembryonic antigen enhances clinical prediction of non-small cell lung cancer. *PLoS One* 10, e0126276.
- Rachidi, S., Wallace, K., Day, T.A., Alberg, A.J., and Li, Z. (2014). Lower circulating

- platelet counts and antiplatelet therapy independently predict better outcomes in patients with head and neck squamous cell carcinoma. *J. Hematol. Oncol.* 7, 65.
27. Lim, M., Park, S., Jeong, H.O., Park, S.H., Kumar, S., Jang, A., Lee, S., Kim, D.U., and Cho, Y.K. (2021). Circulating Tumor Cell Clusters Are Cloaked with Platelets and Correlate with Poor Prognosis in Unresectable Pancreatic Cancer. *Cancers*, 13.
 28. Yu, M., Bardia, A., Wittner, B.S., Stott, S.L., Smas, M.E., Ting, D.T., Isakoff, S.J., Ciciliano, J.C., Wells, M.N., Shah, A.M., et al. (2013). Circulating breast tumor cells exhibit dynamic changes in epithelial and mesenchymal composition. *Science* 339, 580–584.
 29. Hu, M., Yao, J., Carroll, D.K., Weremowicz, S., Chen, H., Carrasco, D., Richardson, A., Violette, S., Nikolskaya, T., Nikolsky, Y., et al. (2008). Regulation of in situ to invasive breast carcinoma transition. *Cancer Cell* 13, 394–406.
 30. Francart, M.E., Lambert, J., Vanwynsberghe, A.M., Thompson, E.W., Bourcy, M., Polette, M., and Gilles, C. (2018). Epithelial-mesenchymal plasticity and circulating tumor cells: Travel companions to metastases. *Dev. Dyn.* 247, 432–450.
 31. Son, H.J., and Moon, A. (2010). Epithelial-mesenchymal Transition and Cell Invasion. *Toxicol. Res.* 26, 245–252.
 32. Semenza, G.L. (2016). The hypoxic tumor microenvironment: A driving force for breast cancer progression. *Biochim. Biophys. Acta* 1863, 382–391.
 33. Zhang, Q., Lu, S., Li, T., Yu, L., Zhang, Y., Zeng, H., Qian, X., Bi, J., and Lin, Y. (2019). ACE2 inhibits breast cancer angiogenesis via suppressing the VEGFa/VEGFR2/ERK pathway. *J. Exp. Clin. Cancer Res.* 38, 173.
 34. Takayama, Y., Hattori, N., Hamada, H., Masuda, T., Omori, K., Akita, S., Iwamoto, H., Fujitaka, K., and Kohno, N. (2016). Inhibition of PAI-1 Limits Tumor Angiogenesis Regardless of Angiogenic Stimuli in Malignant Pleural Mesothelioma. *Cancer Res.* 76, 3285–3294.
 35. Nakayama, A., Roquid, K.A., Iring, A., Strilic, B., Günther, S., Chen, M., Weinstein, L.S., and Offermanns, S. (2023). Suppression of CCL2 angiocrine function by adrenomedullin promotes tumor growth. *J. Exp. Med.* 220, e20211628.
 36. Dumon, S., Walton, D.S., Volpe, G., Wilson, N., Dassé, E., Del Pozzo, W., Landry, J.R., Turner, B., O’Neill, L.P., Göttgens, B., and Frampton, J. (2012). Itga2b regulation at the onset of definitive hematopoiesis and commitment to differentiation. *PLoS One* 7, e43300.
 37. Chen, Y., Zhang, S., Wang, Q., and Zhang, X. (2017). Tumor-recruited M2 macrophages promote gastric and breast cancer metastasis via M2 macrophage-secreted CHI3L1 protein. *J. Hematol. Oncol.* 10, 36.
 38. De Giovanni, M., Tam, H., Valet, C., Xu, Y., Looney, M.R., and Cyster, J.G. (2022). GPR35 promotes neutrophil recruitment in response to serotonin metabolite 5-HIAA. *Cell* 185, 1103–1104.
 39. Pagano, E., Elias, J.E., Schneditz, G., Saveljeva, S., Holland, L.M., Borrelli, F., Karlsen, T.H., Kaser, A., and Kaneider, N.C. (2022). Activation of the GPR35 pathway drives angiogenesis in the tumour microenvironment. *Gut* 71, 509–520.
 40. Donato, C., Kunz, L., Castro-Giner, F., Paasinen-Sohns, A., Strittmatter, K., Szczerba, B.M., Scherrer, R., Di Maggio, N., Heusermann, W., Biehmaier, O., et al. (2020). Hypoxia Triggers the Intravasation of Clustered Circulating Tumor Cells. *Cell Rep.* 32, 108105.
 41. Du, J., Wang, C., Chen, Y., Zhong, L., Liu, X., Xue, L., Zhang, Y., Li, Y., Li, X., Tang, C., et al. (2022). Targeted downregulation of HIF-1alpha for restraining circulating tumor microemboli mediated metastasis. *J. Control. Release* 343, 457–468.
 42. Ge, X., Zhang, W., Zhu, T., Huang, N., Yao, M., Liu, H., Wang, D., Zhu, G., Zhang, Z., and Hu, C. (2021). Hypoxia-activated platelets stimulate proliferation and migration of pulmonary arterial smooth muscle cells by phosphatidylserine/LOX-1 signaling-impelled intercellular communication. *Cell. Signal.* 87, 110149.
 43. Delaney, C., Davison-Castillo, P., Allawzi, A., Posey, J., Gandjeva, A., Neeves, K., Tuder, R.M., Di Paola, J., Stenmark, K.R., and Nozik, E.S. (2021). Platelet activation contributes to hypoxia-induced inflammation. *Am. J. Physiol. Lung Cell Mol. Physiol.* 320, L413–L421.
 44. Kulasinghe, A., Zhou, J., Kenny, L., Papautsky, I., and Punyadeera, C. (2019). Capture of Circulating Tumour Cell Clusters Using Straight Microfluidic Chips. *Cancers* 11, 89.
 45. Sylman, J.L., Mitrugno, A., Tormoen, G.W., Wagner, T.H., Mallick, P., and McCarty, O.J.T. (2017). Platelet count as a predictor of metastasis and venous thromboembolism in patients with cancer. *Converg. Sci. Phys. Oncol.* 3, 023001.

STAR★METHODS

KEY RESOURCES TABLE

REAGENT or RESOURCE	SOURCE	IDENTIFIER
Antibodies		
Anti-pan cytokeratin	Abcam	ab7753
P-Selectin polyclonal antibody	Proteintech	13304-1-AP
CD45R (RA3-6B2)	Santa Cruz	sc-19597
Alexa Fluor 488-labeled goat anti-mouse IgG (H + L)	Proteintech	SA00013-1
594-labeled goat anti-rabbit IgG (H + L)	Proteintech	SA00013-4
TRITIC-labeled goat anti-Rat IgG (H + L)	Proteintech	SA00007-7
CD45 Rabbit Polyclonal antibody	Proteintech	20103-1-AP
FITC anti-mouse CD326 (Ep-CAM)	Biolegend	118207
Alex 594 anti-mouse CD45	Biolegend	103144
Chemicals, peptides, and recombinant proteins		
Fetal bovine serum	ExCell Bio	FSP500
RPMI-1640 medium	HyClone	SH30027.02
DMEM medium	HyClone	SH30022.01B
Trypsin (C0201)	Beyotime	SH30809.01B
Chlorotrimethylsilane (TMCS)	Sigma Aldrich	75-77-4
Sylgard 184 PDMS	Dow Corning	04019862_342
SynperonicpeR/F127	Aladdin	9003-11-6
1×Phosphate buffer saline	Servicebio	P1020
CFSE (carboxyfluorescein succinimidyl amino ester)	eBioscience	65-0850-84
PI (Propidium Iodide)	Sigma Aldrich	P4864
EDTA (Ethylenediaminetetraacetic acid)	Sinopharm	6381-92-6
4% Paraformaldehyde	Solarbio	P1110
0.1% Triton100	Beyotime	P0096
DAPI	Beyotime	C1006
Aspirin	yuanyebio	50-78-2
U46619	yuanyebio	56985-40-1
D-luciferin	YEASEN	40902EC
Deposited data		
RNA-seq data	This paper	GEO:GSE256445

RESOURCE AVAILABILITY

Lead contact

Data are available by request. Correspondence should be addressed to Xiaoxiang Guan, Xin Han and Yanni Song. Email address: xguan@njmu.edu.cn (X.G.), xhan0220@njucm.edu.cn (X.H.), 1525@hrbmu.edu.cn (Y.S.) and Fang Yang yangfangnju@hotmail.com (F.Y.).

Materials availability

This study did not generate any unique new reagent. All reagents used in this study are commercially available.

Data and code availability

- Data: RNA-seq data have been deposited at GEO and are publicly available as of the date of publication. Accession number is GSE256445.
- Code: This paper does not report original code.

- Additional information: Any additional information required to reanalyze the data reported in this paper is available from the [lead contact](#) upon reasonable request.

EXPERIMENTAL MODEL AND STUDY PARTICIPANT DETAILS

Cell culture and preparation

A549 and 4T1 cells were purchased from the American Type Culture Collection, propagated according to manufacturer instructions, cultured under standard conditions of 37°C and 5% CO₂ atmosphere, and grown in RPMI-1640 and DMEM medium (HyClone) supplemented with 10% fetal bovine serum (FBS) respectively and 1% Penicillin-streptomycin. All cell lines were maintained in logarithmic phase of growth. Mycoplasma was tested every 2 weeks. A part of A549 and 4T1 cells were engineered to stably express GFP to intuitively test capture and release performance on the chip. Other parts of 4T1 cells were engineered to stably express luciferase for the *in vivo* image while untagged cells were used for viability experiments that required staining.

Construction of experimental lung metastasis

Four to six-week-old female BALB/c mice were purchased from Huachuang Sino for use in experiments involving drug treatment and/or tumor cell injection. All animal procedures were approved and complied with the guidelines of the Institutional Animal Care Committee of Nanjing University of Chinese Medicine (ethical approval number: 202209A008). 4T1-Luc or/and 4T1 ($1 \times 10^6/100 \mu\text{L}$) cells were injected by tail vein into BALB/c mice after at least 2 weeks can occur a certain of lung metastasis.

Blood samples preparation

The blood samples of BC patients used in this experiment were from the Department of Breast Gland of Jiangsu Provincial People's Hospital People's Hospital, diagnosed as breast cancer by pathology, approved by the Ethics Science Committee of Jiangsu Provincial People's Hospital, obtained with informed consent, and carried out in accordance with the guidelines and protocols of the experiment.

METHOD DETAILS

Chip design and development

The Cluster-Chip pattern was designed using AutoCAD (Autodesk) and is composed of 1024 parallel tracks, each equipped with seven consecutive CTC-cluster traps. Three triangular columns form a basic unit, and tiny holes are formed between the three columns to form a capture network. The depth of the chip with one inlet and one outlet is 100 μm and the distance between the two adjacent triangular columns is 12 μm . The microfluidic device was developed according to standard photolithography and soft lithography procedures. For mold fabrication, SU-8 photoresist (Micro Chem) was spun on a silicon wafer and patterned in the form of microfluidic channels through a chrome photomask by conventional photolithography. Polydimethylsiloxane (PDMS) prepolymer and cross-linker (Sylgard 184, Dow Corning) mixed at a 10:1 ratio was poured onto the mold, degassed, and then cured at 80°C for 30 min. The cured PDMS was peeled off the mold bonds onto a glass substrate. Before bonding, the cured PDMS and the glass were treated with oxygen plasma for 1 min to finish surface activation.

Device operation

The Cluster-Chip was drained of air for 10 min and filled with 1% F127 until the channel was met to avoid nonspecific cell adhesion to the PDMS. A syringe pump was used to introduce solutions into the devices. The pump was loaded with a 5 mL syringe and a plastic TYGON tube containing CTC blood and cell suspensions and connected to the inlet reservoir by a flat steel pin. For the capture experiment, we processed the whole blood/PBS spiked with cell clusters in the chip at 4°C under different flow speeds to screen for the best flow rates for capture. For the recovery experiment, the syringe pump was driven at different rates at 4°C to release captured cells from the Cluster-Chip with the best release efficiency while also maintaining the viability and integrity of cells. Before operating the syringe pump, we connected the plastic TYGON tube in reverse to the outlet as the "inlet" and the original inlet as the "outlet" and connected the tube to separate wells of ultra-low attachment well plates (Corning, Inc.) for subsequent experiments.

Cell-cluster spiking experiments

To generate cell clusters, two main methods were used. One method was done after removal of the media and washing with PBS, with cells subsequently incubated growing in monolayer at 80% confluence with trypsin (Beyotime, C0201) for 1 min with gentle pipetting of cells during trypsinization process to generate floating clusters. The second method involved adding the single cell suspension to the ultra-low attachment well plates for early aggregation. Once there was formation of clusters, the clusters were distributed in ultra-low attachment well plates immediately for subsequent use. The clusters were counted manually from microscopy images and their concentrations were adjusted accordingly. This was followed by pipetting a volume of the cluster suspension spiked into PBS or blood samples from healthy BALB/c mice via cardiac puncture and collected into EDTA-coated microcontainer tubes.

Fluorescent live and dead assays

To detect the viability of the cell clusters after capture and release by the chip, we used eBioscience CFSE cell viability reagent to identify the live cells and PI (Sigma Aldrich, P4864) cell apoptosis reagent to identify the dead cells. Dissolving the above stock solution of fluorescent reagents in PBS at final working concentrations were done according to the instructions. The diluting solutions were then added to the cell cluster suspensions for 10–20 min and the reaction was stopped with cooled FBS. The Cluster-Chip was imaged with an inverted fluorescence microscope (Mshot Guangzhou) before capture and after release. Both of the cell clusters were needed to acquire corresponding fluorescent images to be in contrast with each other.

Blood processing and immunofluorescence staining

Mouse blood was retrieved in EDTA-contained tubes via cardiac puncture of tumor-bearing BALB/c mice. Up to 0.5–1 mL of blood was collected and diluted with filtered 1×PBS. Around 4–5 mL of whole blood samples were collected from breast cancer patients (BC patients) in EDTA vacutainers at multiple time points during disease progression. These samples were used within 4 h after collection and diluted by 1:2 in phosphate buffered saline (PBS) solution. After Cluster-Chip processing of these blood samples, immunofluorescence staining was done by first washing the chips with PBS, fixing them for 30 min with 4% paraformaldehyde (PFA) (Solarbio, P1110), permeabilizing them for 15 min with 0.1% Triton X-100 (Beyotime, P0096), and blocking them for 1 h with 3% bovine serum albumin (BSA) (ExCell Bio, FSP500) at room temperature. A cocktail of primary antibodies including anti-mouse monoclonal Pan-cytokeratin (Abcam, ab7753), anti-rabbit polyclonal P-selectin (Proteintech, 13304-1-AP, or Anti-Rat polyclonal CD45R (RA3-6B2) (Santa Cruz, sc-19597) was used for patient blood samples. Anti-mouse monoclonal Pan-cytokeratin (Abcam, ab7753) and Anti-rabbit polyclonal CD45 (Proteintech, 20103-1-AP) were used for mouse blood samples and were added to the chips and incubated at 4°C for one night. On the second day, the chips were washed and secondary antibodies such as Alexa Fluor 488-labeled goat anti-mouse IgG (H + L) (Proteintech, SA00013-1) and 594-labeled goat anti-rabbit IgG (H + L) (Proteintech, SA00009-2), or TRITIC-labeled goat anti-Rat IgG (H + L) (Proteintech, SA00007-7), were added and kept in the dark for 3 h. After washing, 4,6-diamidino-2-phenylindole (DAPI) (Beyotime, 28718-90-3) was used to stain for 5 min to detect nuclei following washing the chips once again. The cell clusters were imaged using a fluorescence microscope (Mshot Guangzhou) and manually counted. For live staining of CTM for downstream analysis, unfixed cell clusters were stained with FITC anti-mouse CD326 (EPCAM) (118027, Biolegend) and Alex 594 anti-mouse CD45(103144, Biolegend) to identify the captured CTM.

Drug intervention in lung metastases of mice

Aspirin (ASA, Acetylsalicylic acid, 50-78-2, Shanghai Yuanye Bio-Technology Co.) was dissolved in sterile deionized water and resuspended in drinking water at 180 mg/L. U46619 (56985-40-1, Shanghai Yuanye Bio-Technology Co.) was diluted in sterile deionized water and delivered at 50 µg/kg through a 180-mg/L aspirin solution. The mice were divided randomly into 4 groups and treated with vehicle, aspirin, aspirin plus U46619, and U46619, respectively. Two days prior to this, 4T1-Luc (1 × 10⁶/100 µL) cells were injected by tail vein into BALB/c mice and drugs were administered through drinking water that was changed every second day. BLI of live animals was initiated 7 days after cell injection and performed weekly. Two to three mice were scanned at one time to identify any metastatic mouse lungs nodules. After 2–3 weeks of treatment with either vehicle or drugs, blood was collected in EDTA-coated tubes through cardiac puncture of terminally anesthetized mice with 2.5% isoflurane (RWD). BALB/c mice. Mice lungs were harvested and tumor burden was quantified by manual segmentation via ImageJ. The collected mice lungs from each group partly were embedded in paraffin and 5-µm sections were stained by H&E performed by AiFang Biological.

In vivo bioluminescence imaging and tumor progression

In order to investigate for metastasis, BLI of whole mice was initiated 7 days after cell line injection and performed weekly. Mice were injected i.p. with 15 mg/mL of D-luciferin (YEASEN) in PBS, anesthetized with 2.5% isoflurane, and subsequently imaged. Ten minutes following this injection, mice were imaged using a charge-coupled device camera-based BLI system (IVIS Spectrum, PerkinElmer; exposure time: Auto, binning: Medium, field of view: C, f/stop 2, emission filter: open). Signal was measured and recorded as total flux (photons/seconds). Corresponding grayscale photographs and color luciferase images were automatically superimposed and analyzed with Living Image software (PerkinElmer).

RNA extraction library construction and RNA sequencing

The SMART-Seq v4 Ultra Low Input RNA Kit (Clontech, Japan) was used to prepare the low-input library following the procedures below: 1) Preparing the cDNA library; 2) cDNA Purification and size selection (150–300 bp); 3) Preparing sequencing-ready library by adding i5/i7 adaptor using PCR method; 4) Library quality control or assessing the size and concentration of the library using Agilent 2100 Bioanalyzer; 5) Library sequencing was performed on Illumina platforms using a 2x150bp paired-end sequencing protocol. After total RNA was extracted, mRNA was purified from total RNA using Dynabeads Oligo (dT) (Thermo CA, USA) with two rounds of purification. Following purification, the mRNA was fragmented into shorter fragments using divalent cations under elevated temperatures (Magnesium RNA Fragmentation Module [NEB, cat.e6150, USA] under 94°C for 5–7 min). The cleaved RNA fragments were reverse-transcribed to create cDNA using SuperScriptII Reverse Transcriptase (Invitrogen, cat. 1896649, USA). This was next used to synthesize U-labeled second-stranded DNA with E. coli DNA polymerase I (NEB, cat.m0209, USA), RNase H (NEB, cat.m0297, USA) and dUTP Solution (Thermo Fisher, cat.R0133, USA). An A-base was

then added to the blunt ends of each strand, preparing them for ligation to the indexed adapters. Each adapter contained a T-base overhang for ligating the adapter to the A-tailed fragmented DNA. Dual-index adapters were ligated to the fragments and size selection was performed with AMPureXP beads. After heat-labile UDG enzyme (NEB, cat.m0280, USA) treatment of the U-labeled second-stranded DNA, the ligated products were amplified with PCR by the following conditions: initial denaturation at 95°C for 3 min; 8 cycles of denaturation at 98°C for 15 s, annealing at 60°C for 15 s, extension at 72°C for 30 s; and final extension at 72°C for 5 min. The average insert size for the final cDNA libraries were 300 ± 50 bp. Finally, we performed 2×150 bp paired-end sequencing (PE150) on an Illumina Novaseq 6000 (LC-Bio Technology CO., Ltd., Hangzhou, China) following the vendor's recommended protocol.

Bioinformatics pipeline

Cutadapt software (<https://cutadapt.readthedocs.io/en/stable/>, version: cutadapt-1.9) was used to remove the reads that contained adaptor contamination. After removal of low-quality bases and undetermined bases, we used HISAT2 software (<https://daehwankimlab.github.io/hisat2/>, version: hisat2-2.0.4) to map reads to the genome (i.e., Homo sapiens Ensembl v96). The mapped reads of each sample were assembled using StringTie (<http://ccb.jhu.edu/software/stringtie/>, version: stringtie-1.3.4days). Expression levels of all transcripts were estimated and performed as calculating FPKM (FPKM = [total exon fragments/mapped reads (millions) \times exon length (kB)]). The differentially expressed mRNAs were selected with fold change >2 or fold change <0.5 and p value <0.05 by edgeR (<https://bioconductor.org/packages/release/bioc/html/edgeR.html>). Gene ontology terms (<http://www.geneontology.org/>) and KEGG pathways (<http://www.genome.jp/kegg/>) of these differentially expressed mRNAs were also annotated.

qPCR reaction

qPCR validation was performed on the samples returned from the experimental and control sequencing groups. Each well had 0.4 μ L of upstream and downstream primers, 4.2 μ L of enzyme-free water, 5 μ L of cDNA template, and 10 μ L of $2\times$ Taq Pro Universal SYBR qPCR Master Mix. After the sample spotting was completed, a transparent sealing film was applied and the program was set on the machine (CFX96, Bio-rad; preheat 95°C for 3 min, amplification 95°C for 10 s, 60°C for 30 s for 40 cycles of amplification), The primer sequences are shown in Table S4.

Hypoxia experiments

4T1 cells were inoculated in low adherence 12-well plates at a density of approximately 50–100 cells per well. The experiments were divided into four groups: platelets co-cultured with tumor cells in a hypoxia environment for 24 h, platelets co-cultured with tumor cells in a normoxic environment for 24 h, tumor cells alone in a hypoxia environment for 24 h, and tumor cells alone in a normoxic environment for 24 h. Platelets were isolated from normal mice and were added as 50 μ L aliquots of platelet solution (5×10^7) into each well. 100 μ M CoCl₂ was added to the cell culture medium to simulate a hypoxia environment.

QUANTIFICATION AND STATISTICAL ANALYSIS

The data were analyzed using Graphpad Prism 8.0.2. The t-test or nonparametric test was used for the comparison of two independent samples and one-way ANOVA or nonparametric test was used for the comparison of multiple independent samples. The counting data was tested by χ^2 or the Fisher exact test. The correlation analysis between CTM and platelet, serum fibrinogen, and D-dimer levels was carried out by Spearman rank correlation method with $p < 0.05$ indicating statistical significance, * $p < 0.05$, ** $p < 0.01$, *** $p < 0.001$. All experiments were repeated at least three times.